Rotor Dynamics in One and Two Dimensions

Abhimanyu Nowbagh (MS16070)

A dissertation submitted for the partial fulfilment of BS-MS dual degree, under the supervision of

Dr. Abhishek Chaudhuri, IISER Mohali

Department of Physics
Indian Institute of Science Education Research
India

May 2021

Certificate of Examination

This is to certify that the dissertation titled "Rotor dynamics in one and two dimensions" submitted by Mr. Abhimanyu Nowbagh (Reg. No. MS16070) for the partial fulfilment of BS-MS dual degree programme of the institute, has been examined by the thesis committee duly appointed by the institute. The committee finds the work done by the candidate satisfactory and recommends that the report be accepted.

Dr. Abhishek Chaudhuri (Supervisor)

Dr. Dipanjan Chakraborty

Dr. Sanjeev Kumar

Dated: 29.05.2021

Declaration

The work presented in this dissertation has been carried out by me under the guidance of Dr. Abhishek Chaudhuri at the Indian Institute of Science Education and Research Mohali.

This work has not been submitted in part or in full for a degree, a diploma, or a fellowship to any other university or institute. Whenever contributions of others are involved, every effort is made to indicate this clearly, with due acknowledgement of collaborative research and discussions. This thesis is a bonafide record of original work done by me and all sources listed within have been detailed in the bibliography.

Abhimanyu Nowbagh
(Candidate)
Dated:
29/5/21

In my capacity as the supervisor of the candidate's project work, I certify that the above statements by the candidate are true to the best of my knowledge.

Dr. Abhishek Chaudhuri
(Supervisor)

Acknowledgement

During this year of my MS-thesis, and overall five years at IISER Mohali, there have been numerous people who have helped me and given me support.

I would like to thank Dr. Abhishek Chaudhuri. His guidance and insightful discussions have helped me a lot throughout my thesis, and also inspired me to develop a deeper interest in this field of soft matter. I also thank my committee members Dr. Dipanjan Chakraborty and Dr. Sanjeev Kumar for their inputs and further suggestions to the work.

I want to thank DST Inspire for providing financial support. I would also like to acknowledge IISER Mohali and it's Library specially, for providing books, resources and facilities. I thank Subhashree for letting me use her device for running computations.

I am grateful to Nitish, whose conversations helped regain my love and curiosity for physics. I would like to thank my friends Abhijeet, Anshul, Ijaz, Kimaya, Kusha, Mayank, Sasank, Satender, Shikhar, Srinivas and Vinod without whom life in IISER would not have been a significant one.

I am indebted to my family, for the love and support they have given me throughout my life decisions.

Abhimanyu Nowbagh

Contents

List of Figures

Abstract

A classical 1-D chain of rotors mimicking Non-Newtonian fluids and showing different flow regimes under different parameters is reproduced [Eva+15]. The ends of the 1-D rotor system are rotated in opposite directions, and it is seen that the phase behaviour is analogous to a complex fluid system, with the angular velocity distribution of the rotors representing the shear flow in fluids. Then upon increasing the dimension, a 2D system of rotors with an added hydrodynamic interaction is studied as a model for bacterial carpets. Each rotor has an intrinsic angular velocity, and also subjects a force on the surrounding fluid, which leads to synchronization and spirals formation in the fluid flow under different cases[UG10].

Chapter 1

Introduction

The classical XY model, like the Ising model, is a lattice spin model initially developed to study magnetic systems and equilibrium phase transitions in them [Kos74]. The XY model has a spin $s_j = (\cos\theta_j, \sin\theta_j)$ at each lattice site j, which is allowed to rotate in a plane, where θ_j can take values between $-\pi < s_j < \pi$. However, it was later seen that these models could be used as models to study phenomena far away from magnetic systems too[TT95; LG85].

1.1 Microfluidics and Bacterial Carpets

Microfluidics refer to the control and manipulation of fluid flow in the small (∼micro) scale, where the surface forces dominate over the volume forces. When active particles like micropumps or microorganisms are used, it is termed as active microfluidics.

Darnton et al. performed experiments with a system of "bacterial carpets", with the head of the bacteria embedded on a substrate and the flagella left to rotate in the surrounding fluid[Dar+04]. The flagella could coordinate the flow of the fluid forming linear and rotational flows. Bacteria and similar microorganisms have benefits of being used as microfluidic mixers: the cost of power source to run the microfluidic mixers is reduced, and self-replication of the bacteria within the medium removes the cost of wear and tear and replacement of mechanical microfluidic rotors.

It cannot be overlooked that a system of embedded bacteria with their heads fixed, is just essentially a system of rotors in a fluid. Thus a classical XY model can be used to model this system, with the rotors acting as substitutes to the bacteria. Computational simulation and analysis of such models can lead to better understanding of the fluid flow characteristics due to microfluidic mixers. Such an array of rotors coupled with hydrodynamic interaction was studied by Uchida and Golestanian [UG10], and part of my work in this thesis is based on this paper.

1.2 1-D XY model and non-Newtonian phenomena

Before working on the problem of bacterial carpets, I started looking at 1-D classical XY models. An interesting phenomenon was seen where the classical 1-D XY model under angular momentum conserving Langevin dynamics, showing phase behaviour which could be drawn analogous to the behaviour of non-Newtonian fluids.

1.2.1 Non-Newtonian Fluids

Unlike Newtonian fluids where under uniform stress, shear flow is evenly distributed throughout the fluid, non-Newtonian fluids show uneven distribution of shear-flow, in the process forming macroscopic regions with distinct shear rates. These non-Newtonian fluid flow transitions have been observed in various complex-fluids like foams, polymers, surfactant solutions and dense colloids[KD08; Haw04; Kun+12; SMC03].

Newton's law of viscosity states there exists a linear relation between shear stress(τ) and rate of shear(du/dy), where u is the velocity of the fluid :

$$\tau = \mu \frac{du}{dy}$$

Fluids which don't follow this relation are classified as non-Newtonian fluids. These fluids don't have a constant viscosity, rather their viscosity depends on the shear stress applied.

1.3 Organization of the Thesis

Since the 1-D XY model and its analogy to the non-Newtonian fluid behaviour was interesting enough, I initially studied this system in detail. Under different initial conditions for the 1-D XY model pushed out of equilibrium, four different phase behaviour analogous to the flow regimes for non-Newtonian fluids were observed:

- Uniform flow
- Shear Banded flow
- Solid-Fluid coexistence
- Slip-Plane regime

A theoretical analysis was also presented which finally leads to a constitutive relation for the fluid. All these have been discussed in Chapter 2.

Subsequently, I worked on a 2-D system of rotors with an added hydrodynamic interaction to simulate the bacterial carpet system. Various flow behaviours were observed upon changing the geometric frustration in the fluid due to the rotors:

- Global synchronization
- Self-proliferating spiral waves
- Complete disorder.

This part has been discussed in Chapter 3. With the computational basis and surety of the results, this work can be taken further with the introduction of free swimmers in the fluid: rotors free to move around in the fluid, with an added excluded volume interaction.

Chapter 2

1-D Chain of Rotors

2.1 Model and Dynamics

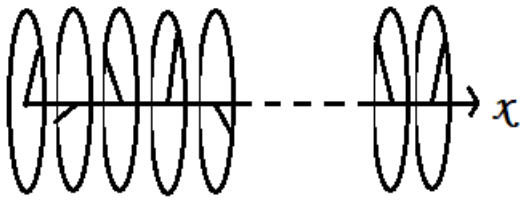

Figure 2.1: 1-D chain of rotors.

The rotors are placed in a 1-D chain with the plane of rotors perpendicular to the axis of the chain as shown in Fig(2.1). The only degree of freedom of the system is the angle of the j^{th} spin θ_j. There is only nearest neighbour interaction, therefore the Hamiltonian becomes:

$$H = \sum_{i=1}^{N} [-s_j.s_{j-1} + \frac{1}{2}\dot{\theta_j}^2] \tag{2.1}$$

The first term of the Hamiltonian is the interaction energy between the nearest neighbour rotors. The (-) sign is such that the rotors tend to align parallel in the ground state. The second term is the kinetic energy (angular) of the rotor. The moment of inertia of the rotors has been taken to be unity.

In equilibrium, the model has trivial behaviour with a single transition to an ordered state at zero temperature [Mat84]. For checking non-equilibrium properties, Langevin dynamics is introduced. Newton's third law is obeyed, and angular momentum is

conserved. The equations of motion are:

$$\ddot{\theta_j} = \tau_j - \tau_{j-1} \tag{2.2}$$

$$\tau_j = \sin \Delta\theta_j + \mu \Delta\dot{\theta_j} + \eta_j(t) \tag{2.3}$$

Here τ_j is the torque on the j^{th} rotor, $\Delta\theta_j$ is the angular difference between $(j+1)^{th}$ and j^{th} rotor. μ is the friction coefficient between the rotors and η_j is delta-correlated noise at temperature T with zero mean and variance given by,

$$< \eta_i(t)\eta_j(t') >= 2\mu T\delta(t-t')\delta_{ij}. \tag{2.4}$$

The system is driven into non-equilibrium by rotating the end rotors in opposite directions (giving it a "twist"). This induces rotation throughout the rotor system. The rotor system is compared to a fluid flow with the slope of the angular velocity of the rotors analogous to the shear rate throughout the fluid. The initial twist represents the shear stress applied. If the rotors start rotating together, they resemble a solid region (having no shear flow).

2.2 Simulation

The simulation was performed for $N = 1024$ rotors. The values of temperature (T), coefficient of friction (μ), and twist rate ($\dot{\gamma}$) are changed to obtain different flow behaviour.

The second order differential equation Eq.(2.2) is broken into two first order differential equations for angular velocity and angular position respectively and are evolved using the Runge-Kutta Fourth Order algorithm. The first and last rotors keep rotating with an angular offset of $N\dot{\gamma}$.

2.3 Flow Behaviour Observed

Varying the Temperature (T), friction coefficient (μ), and global shear rate ($\dot{\gamma}$), leads to different flow behaviour as observed for Non-Newtonian fluids.

1. Uniform Flow

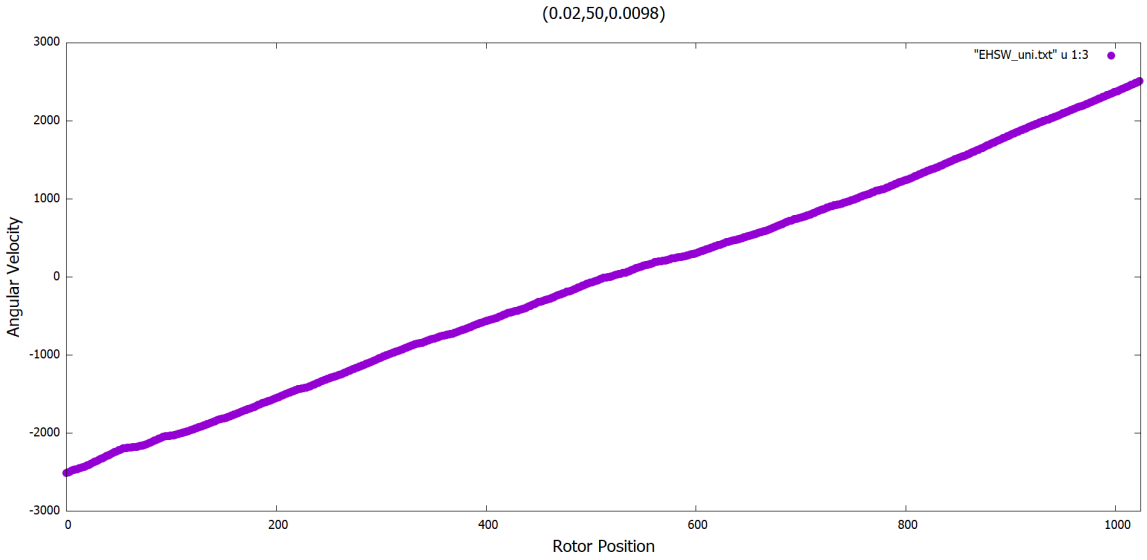

Figure 2.2: Uniform Flow.($T = 0.02$, $\mu = 50$, $\dot{\gamma} = 0.0098$)

The flow is as expected of Newtonian fluids, the shear is evenly spread throughout the system. In terms of the fluid analogy, the entire system has constant viscosity. Here, the global shear rate is equal to the local shear rate throughout the fluid. ($\dot{\gamma} = s_j$)

2. Shear Banding Flow

Here, the system of rotors starts showing non-Newtonian flow behaviour. The shear flow is unevenly distributed throughout the system. Different macroscopic regions show different effective viscosities.

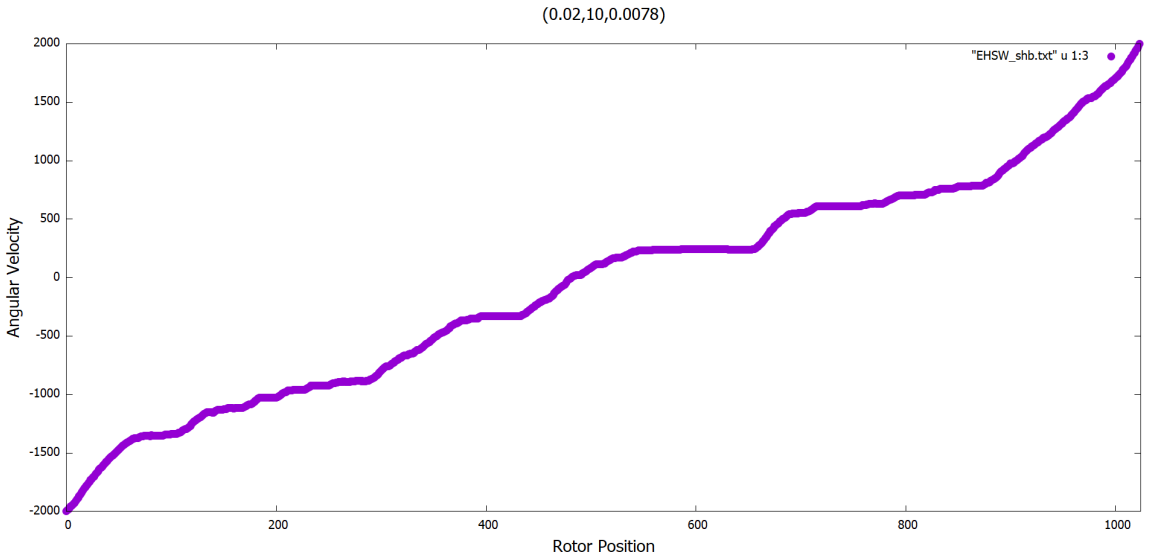

Figure 2.3: Shear Banded Flow. ($T = 0.02$, $\mu = 10$, $\dot{\gamma} = 0.0078$)

3. Solid Fluid Coexistence

   The system arranges in regions with $s_j = 0$ (solid regions), where sections of the rotors rotate together with $\Delta\theta = 0$. Between these segments of solid regions rotating at different angular velocities, some shear flow is seen. These are similar to fluid regions with a high shear rate (low viscosity). Hence this phase, can be thought of as a solid-fluid coexistence. It can be seen in Fig(2.4).

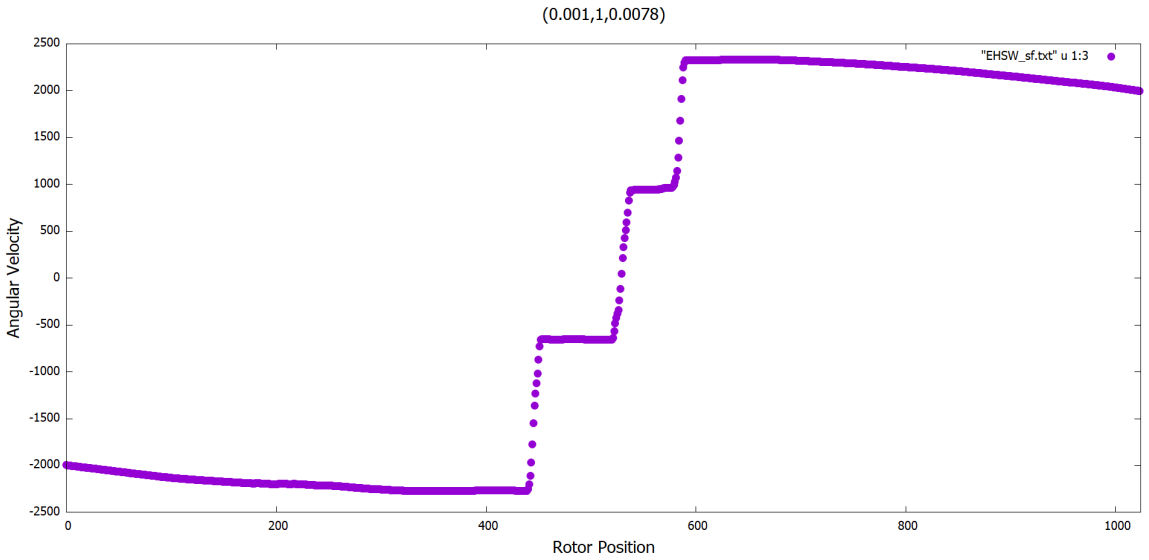

Figure 2.4: Solid-Fluid Coexistence.($T = 0.001$, $\mu = 1$, $\dot{\gamma} = 0.0078$)

4. Slip Plane Regime

   The low viscosity fluid regions from the previous phase completely disappear and the system gets divided into different solid regions rotating at different angular

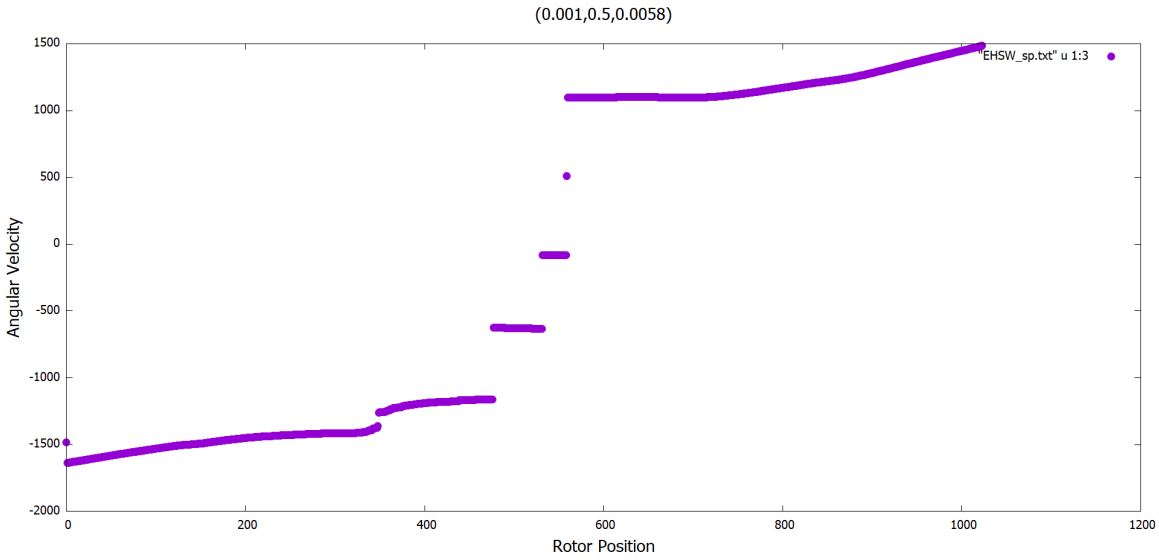

Figure 2.5: Slip-plane regime. $(T = 0.001, \mu = 0.5, \dot{\gamma} = 0.0058)$

velocities. These solid regions are termed as "slip-planes".

The general trend observed is that as temperature and frictional coefficient is decreased, the system transitions from a uniform flow to the slip plane regime. This is because at higher values of friction and temperature, the $\mu\Delta\dot{\theta}_j$ and $\eta_j(t)$ term dominates over the interaction term $\sin\Delta\theta_j$ in Eq.(2.3). Intuitonally, it can be seen as the high friction coefficient between the rotors tend to make the rotors move together. The high temperature term averages over the structure due to the interaction potential, leading to a uniform flow pattern.

2.4 Inter-Rotor Potential

The inter-rotor potential given by

$$U(\Delta\theta) = -\cos(\Delta\theta)$$

has been plotted for the slip plane regime, solid-fluid coexistence and shear banded state. The dark regions denote higher potential for the adjacent rotors to overcome. Time increases vertically in the following plots.

- Slip-plane regime

  It can be seen that there are four high-potential lines corresponding to the edges of each slip-plane in Fig(2.5). Rest of the plot comprises of low potential regions between the rotors which are easily overcome such that the rotors start rotating

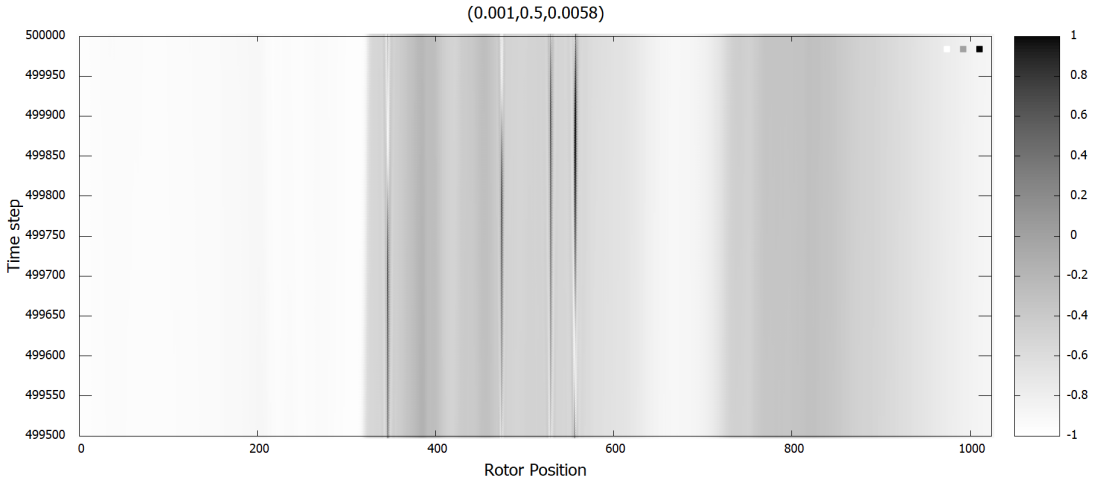

Figure 2.6: Inter-rotor Potential for slip-plane.

together. Low potentials between the rotors give rise to the formation of slip-planes ($s_j = 0$ region).

- Solid-Fluid Coexistence

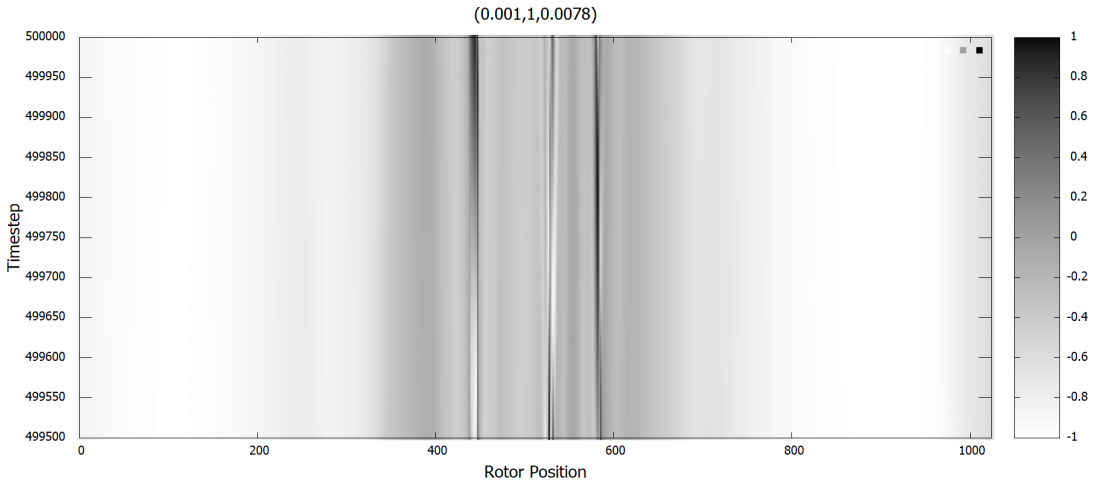

Figure 2.7: Inter-rotor potential for solid fluid coexistence regime.

The high potential yielding regions are broader, corresponding to the low viscosity fluid regions between the slip-planes in Fig(2.4). Similar to the Fig(2.6), the low potential regions let the rotors rotate together giving rise to slip-planes.

- Shear Banding Flow

  There are not many broad low potential regions between the rotors discouraging presence of a slip-plane. Shear is distributed amongst the rotors due to the

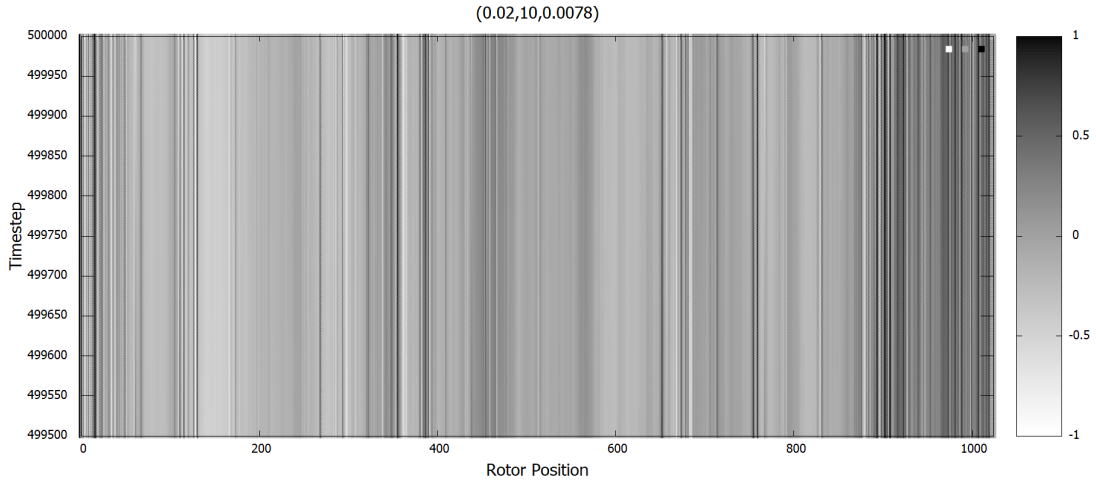

Figure 2.8: Inter-Rotor Potential for a shear banded state

presence of significant potentials throughout the system. However the potentials are of varying magnitude, which does not allow the shear to be evenly spread out too, as seen in the angular velocity distribution in Fig(2.3).

2.5 Theoretical Analysis

Combining Eq.(2.2) for θ_j and θ_{j+1}, and using $\Delta\theta_j = \theta_{j+1} - \theta_j$,

$$\frac{d^2\Delta\theta_j}{dt^2} = \tau_{j+1} + \tau_{j-1} - 2\tau_j \tag{2.5}$$

This equation and Eq.(2.3), form a closed set of equations for $\Delta\theta_j$. Time averaging Eq.(2.5), and using the condition that time-averaged angular acceleration must vanish since there is no external torque gives,

$$< \tau_{j+1} - \tau_j > = < \tau_j - \tau_{j-1} > = constant \tag{2.6}$$

Here $< ... >$ means a temporal average.

Time-averaging Eq.(2.3) gives,

$$\bar{\tau} = < \sin\Delta\theta_j > + \mu s_j \tag{2.7}$$

Here $s_j \equiv < \dot{\Delta\theta_j} >$, $\bar{\tau}$ is the mean torque.

If the first term of the RHS in Eq.(2.7) vanishes, we are left with a Newtonian fluid, with viscosity μ. However due to noise in the system, $< \sin\Delta\theta_j >$ becomes non-zero,

leading to non-Newtonian fluid behaviour. Eq.(2.5) and Eq.(2.3) are non-linear in $\Delta\theta_j$. We will try to linearize it, and find a constitutive relation for the fluid.

We can write $\Delta\theta_j$ as a combination of the shear rate s_j, a constant offset c_j and a fluctuating term with zero mean $\epsilon_j(t)$,

$$\Delta\theta_j = s_j t + c_j + \epsilon_j(t) \tag{2.8}$$

Putting this in Eq.(2.5), leads to:

$$\frac{d\Delta\theta_j}{dt} = s_j + \dot{\epsilon_j}(t)$$

$$\frac{d^2\Delta\theta_j}{dt^2} = \ddot{\epsilon_j}(t)$$

$$\ddot{\epsilon_j}(t) = \tau_{j+1} + \tau_{j-1} - 2\tau_j \tag{2.9}$$

Also Putting Eq.(2.8) in Eq.(2.3) gives,

$$\tau_j = \sin(s_j t + c_j + \epsilon_j(t)) + \mu(s_j + \dot{\epsilon_j}(t)) + \eta_j(t) \tag{2.10}$$

Now time-averaging Eq.(2.10) gives,

$$\bar{\tau} = < \sin(s_j t + c_j + \epsilon_j(t)) > + \mu s_j \tag{2.11}$$

Now we expand $\epsilon_j(t)$ and $\tau_j(t)$ in Fourier modes, with $\hat{\epsilon_j}(\omega)$ and $\hat{\tau_j}(\omega)$ as the respective Fourier coefficients,

$$\epsilon_j(t) = \sum_{\omega} \hat{\epsilon_j}(\omega) e^{i\omega t} \tag{2.12a}$$

$$\tau_j(t) = \sum_{\omega} \hat{\tau_j}(\omega) e^{i\omega t} \tag{2.12b}$$

Inverse Fourier transformations can be applied to find the Fourier coefficients as:

$$< e^{-i\omega t}\epsilon_j(t) > = \sum_{\omega'} \hat{\epsilon_j}(\omega') < e^{i(\omega'-\omega)t} >$$

Since $< e^{i\omega t} > = \delta(\omega, 0)$, where δ is the Kronecker delta function. This leads to:

$$< e^{-i\omega t}\epsilon_j(t) > = \hat{\epsilon_j}(\omega) \tag{2.13}$$

The first Fourier coefficients of $\hat{\epsilon_j}(t)$ and $\hat{\tau_j}(t)$ are their respective means.

$$\hat{\epsilon_j}(0) = 0$$

$$\hat{\tau_j}(0) = \bar{\tau}$$

Now we place this Fourier expansion in the equations of motion, Eq.(2.9) and Eq.(2.10). Eq(2.9) gives,

$$\frac{d^2}{dt^2}(\sum_\omega \hat{\epsilon_j}(\omega)e^{i\omega t}) = \sum_\omega \hat{\tau_{j+1}}(\omega)e^{i\omega t} + \sum_\omega \hat{\tau_{j-1}}(\omega)e^{i\omega t} - 2\sum_\omega \hat{\tau_j}(\omega)e^{i\omega t}$$

The double derivative comes out as,

$$\frac{d^2}{dt^2}(\sum_\omega \hat{\epsilon_j}(\omega)e^{i\omega t}) = -\omega^2 \sum_\omega \hat{\epsilon_j}(\omega)e^{i\omega t}$$

Taking out the summation, and cancelling $e^{i\omega t}$ from both sides gives,

$$-\omega^2\hat{\epsilon}_j(\omega) = \hat{\tau}_{j+1}(\omega) + \hat{\tau}_{j-1}(\omega) - 2\hat{\tau}_j(\omega) \tag{2.14}$$

To find $\hat{\tau}_j(\omega)$, we calculate $< e^{-i\omega t}\tau_j(t) >$,

$$\begin{aligned}\hat{\tau_j}(\omega) =& < e^{-i\omega t}\tau_j(t) > = < e^{-i\omega t}\sin(s_j t + c_j + \epsilon_j(t)) > \\ &+ < e^{-i\omega t}\mu s_j > + < e^{-i\omega t}\mu\dot{\epsilon_j}(t) > + < e^{-i\omega t}\eta_j(t) >\end{aligned} \tag{2.15}$$

Till here, the equations are exact. Now, to linearize, we take the small fluctuation limit, $\epsilon_j(t) << 1$, and write the sin term as $\sin(A+B)$, $\sin[(s_j t + c_j) + \epsilon_j(t)]$ and expand it.

$$\begin{aligned}\hat{\tau_j}(\omega) = \mu s_j\delta(\omega,0) + \hat{\eta_j}(\omega) + i\mu\omega\hat{\epsilon_j}(\omega) + < e^{-i\omega t} \\ [\sin(s_j t + c_j)\cos(\epsilon_j(t)) + \cos(s_j t + c_j)\sin(\epsilon_j(t))] >\end{aligned} \tag{2.16}$$

For small $\epsilon_j(t)$, $\sin(\epsilon_j(t)) \approx \epsilon_j(t))$ and $\cos(\epsilon_j(t)) \approx 1$,

$$\begin{aligned}< e^{-i\omega t}\sin(s_j t + c_j + \epsilon_j(t)) > =& < e^{-i\omega t}\sin(s_j t + c_j) > + \\ & < e^{-i\omega t}\cos(s_j t + c_j)\epsilon_j(t) >\end{aligned}$$

Using $\sin(x) = \frac{e^{ix} - e^{-ix}}{2i}$, and $\cos(x) = \frac{e^{ix} + e^{-ix}}{2}$,

$$\begin{aligned}< e^{-i\omega t}\sin(s_j t + c_j) > &= < e^{-i\omega t}\frac{e^{i(s_j t + c_j)} - e^{-i(s_j t + c_j)}}{2i} > \\ &= \frac{1}{2i}e^{ic_j} < e^{-i\omega t}e^{is_j t} > - \frac{1}{2i}e^{-ic_j} < e^{-i\omega t}e^{-is_j t} > \\ &= \frac{1}{2i}e^{ic_j}\delta(\omega, s_j) - \frac{1}{2i}e^{-ic_j}\delta(\omega, -s_j)\end{aligned}$$

Similarly for $< e^{-i\omega t}\cos(s_j t + c_j)\epsilon_j(t) >$,

$$\begin{aligned} < e^{-i\omega t}\cos(s_j t + c_j)\epsilon_j(t) > &= < e^{-i\omega t}\frac{e^{i(s_j t + c_j)} + e^{-i(s_j t + c_j)}}{2}\epsilon_j(t) > \\ &= \frac{1}{2}e^{ic_j} < e^{i(s_j-\omega)t}\epsilon_j(t) > + \frac{1}{2}e^{-ic_j} < e^{-i(s_j+\omega)t}\epsilon_j(t) > \\ &= \frac{1}{2}e^{ic_j}\hat{\epsilon_j}(\omega - s_j) + \frac{1}{2}e^{-ic_j}\hat{\epsilon}_j(s_j + \omega) \end{aligned}$$

Since $\epsilon_j(t)$ is real valued, it's Fourier coefficients must satisfy: $\hat{\epsilon}_j(-\omega) = \hat{\epsilon}_j^*(\omega)$ Now using $b_j \equiv e^{ic_j}$, and substituting the expressions obtained in Eq.(2.16),

$$\begin{aligned} \hat{\tau_j}(\omega) = \mu s_j \delta(\omega, 0) + \hat{\eta_j}(\omega) + i\mu\omega\hat{\epsilon_j}(\omega) + \frac{1}{2i}b_j\delta(\omega, s_j) \\ -(1/2i)b_j^*\delta(\omega, -s_j) + \frac{1}{2}b_j\hat{\epsilon_j}(\omega - s_j) + \frac{1}{2}b_j^*\hat{\epsilon}_j(s_j + \omega) \end{aligned} \tag{2.17}$$

Thus we have obtained an expression for the Fourier coefficient of torque. To find the mean torque we find $\hat{\tau_j}(0)$.

$$\bar{\tau} = \mu s_j + \frac{1}{2i}(b_j - b_j^*)\delta(s_j, 0) + \frac{1}{2}b_j\hat{\epsilon_j}(-s_j) + \frac{1}{2}b_j^*\hat{\epsilon}_j(s_j)$$

$$\implies \bar{\tau} = \mu s_j + \sin(c_j)\delta(s_j, 0) + \frac{1}{2}b_j\hat{\epsilon_j}(-s_j) + \frac{1}{2}b_j^*\hat{\epsilon}_j(s_j) \tag{2.18}$$

The first term in the expression denotes the Newtonian viscosity, the second term denotes the torque for a solid region of the chain ($s_j = 0$). The final two terms give rise to the non-Newtonian fluid flow.

2.5.1 Mean field analysis

Applying mean-field hypothesis on Eq.(2.14), we replace the torque on the $(j+1)$ and $(j-1)$ rotor by the mean torque $\bar{\tau}$ (zero frequency component of the torque).

$$\omega^2\hat{\epsilon_j}(\omega) = 2\hat{\tau_j}(\omega) - 2\bar{\tau}\delta(\omega, 0) \tag{2.19}$$

Since now we are only concerned with the j^{th} rotor, there exists only a single shear rate, $s = s_j$. Two new coefficients are introduced:

$$a_n \equiv \hat{\epsilon_j}(ns)$$

$$\zeta_n \equiv \hat{\eta_j}(ns)$$

It is also visible that $a_0 = \zeta_0 = 0$ since $\hat{\epsilon}(0) = \hat{\eta}(0) = 0$ and $a_{-n} = a_n^*$, since $\epsilon_j(t)$ is a

real function.

Substituting this in Eq.(2.18),

$$\bar{\tau} = \frac{1}{2}i(b_j^* - b_j)\delta(s,0) + \mu s + \frac{1}{2}b_j a_{-1} + \frac{1}{2}b_j^* a_1$$

Now, if $s_j \neq 0$, c_j can be arbitrarily taken to be zero. This gives $b_j = 1$. Hence,

$$\bar{\tau} = \sin(c_j)\delta(s,0) + \mu s + \Re(a_1) \tag{2.20}$$

For non-zero s_j, Eq.(2.19) gives,

$$(ns)^2\hat{\epsilon_j}(ns) = 2\hat{\tau_j}(ns) - 2\bar{\tau}\delta(n,0)$$

Now using the expression for $\hat{\tau_j}(\omega)$ from Eq.(2.17) gives,

$$\begin{aligned}\implies (ns)^2 a_n = 2[\mu s\delta(n,0) + \zeta_n + i\mu(ns)a_n - \frac{1}{2}ib_j\delta(n,1) + \\ \frac{1}{2}ib_j^*\delta(n,-1) + \frac{1}{2}b_j a_{n-1} + \frac{1}{2}b_j^* a_{n+1}] - 2\bar{\tau}\delta(n,0)\end{aligned}$$

$$\begin{aligned}\implies ns(ns - 2i\mu)a_n = 2(\mu s - \bar{\tau})\delta(n,0) + i\delta(n,-1) - \\ i\delta(n,1) + 2\zeta_n + a_{n-1} + a_{n+1}\end{aligned} \tag{2.21}$$

Taking $n = 1$, and averaging over the noise term gives,

$$s(s - 2i\mu)a_1 = -i + a_2$$

$$\implies a_1 = \frac{i}{\frac{a_2}{a_1} - s(s - 2i\mu)} \tag{2.22}$$

If $R_n \equiv \frac{a_n}{a_{n-1}}$, for $n > 1$

$$ns(ns - 2i\mu)a_n = a_{n-1} + a_{n+1}$$

$$\implies \frac{1}{R_n} = ns(ns - 2i\mu) - R_{n+1} \tag{2.23}$$

Now R_1 can be defined as,

$$R_1 = \frac{1}{s(s - 2i\mu) - R_2}$$

Writing subsequent expressions for R_2, R_3 leads to,

$$R_1 = \frac{1}{s(s - 2i\mu) - \frac{1}{2s(2s-2i\mu) - \frac{1}{3s(3s-2i\mu) - \frac{1}{\cdots}}}} \tag{2.24}$$

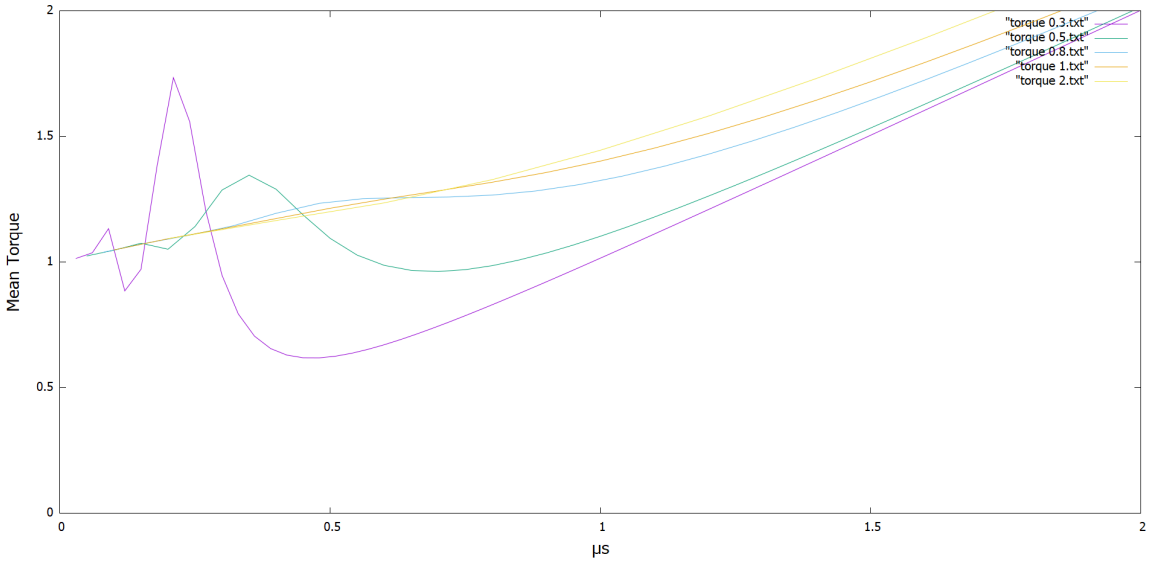

Figure 2.9: Mean torque plotted according to the constitutive relation.

Now, $R_2 = \frac{a_2}{a_1}$. Comparing the definition of R_1 with Eq.(2.22), we find:

$$R_1 = ia_1$$

Putting this in Eq.(2.20),

$$\bar{\tau} = \sin(c_j)\delta(s, 0) + \mu s + \Im(R_1) \tag{2.25}$$

This gives the constitutive relation for our fluid. Plots for $\bar{\tau}$ vs μs for various values of μ is shown in Fig(2.9). R_1 has been calculated till 100 terms. If $s = 0$, from Eq.(2.20), $\bar{\tau} < 1$. So only those values of μ for which the curve goes below 1 in Fig.(2.9) ($\mu \leq 0.5$), allow solid-fluid coexistence and slip-planes.

Chapter 3

2-D Carpet of Rotors

3.1 Model and dynamics

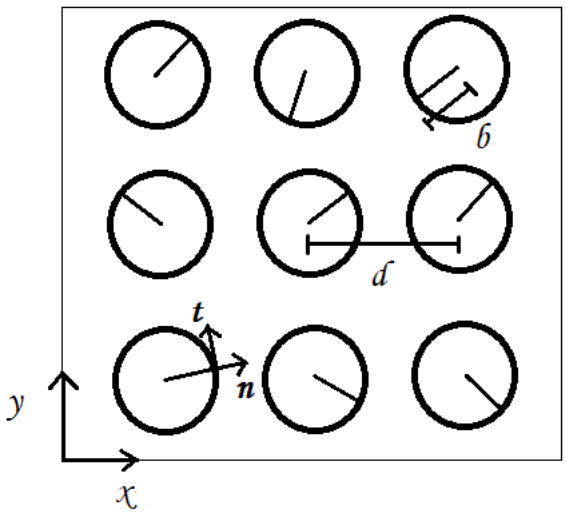

Figure 3.1: Rotors in a 2D plane.

The rotors are placed on a plane, their heads fixed at lattice points distance d apart, and their arms left free to rotate. The length of the rotor arms are b ($b << d$). While rotating they also exert force $\mathbf{F}_i$ on the surrounding fluid, which combines with the hydrodynamic interaction between the rotors. The instantaneous position of the rotor end is:

$$\mathbf{r_i} = \mathbf{r_{0i}} + b\mathbf{n_i} \tag{3.1}$$

Here $\mathbf{r_{0i}}$ is the position of the fixed head, and $\mathbf{n_i}$ is the vector which points along the orientation of the rotor arm as shown in Fig(3.1). If ϕ_i is the angle the i^{th} rotor makes with the x-axis,

$$\mathbf{n}_i = (\cos\phi_i, \sin\phi_i)$$

The velocity of each rotor:

$$\mathbf{v}_i = \frac{d\mathbf{r}_i}{dt} = b\frac{d\mathbf{n}_i}{dt}$$

$$\frac{d\mathbf{n}_i}{dt} = \frac{d(\cos\phi_i, \sin\phi_i)}{dt} = \frac{d\phi_i}{dt}(-\sin\phi_i, \cos\phi_i)$$

If $(-\sin\phi_i, \cos\phi_i) = \mathbf{t}_i$, which points along the tangential direction of the rotor arm,

$$\mathbf{v}_i = b\frac{d\phi_i}{dt}\mathbf{t}_i \tag{3.2}$$

The force exerted by the rotor arm of the i^{th} rotor on the fluid can be broken into radial and tangential components.

$$\mathbf{F_i} = F_n\mathbf{n}_i + F_t\mathbf{t}_i \tag{3.3}$$

F_n and F_t are the radial and tangential components respectively. Varying δ, the angle between $\mathbf{n}_i$ and $\mathbf{F}_i$, leads to varying properties between synchronization, spiral formation and complete disorder.

Now we need to find how the force exerted by a rotor on the fluid influences the rest of the rotor velocities. Herein enters the Blake-Oseen Tensor $\mathbf{G}$, which describes the hydrodynamic interaction at a boundary of a fluid with no-slip condition due to a point force [Bla71]. The velocity field of the fluid can be calculated now as

$$\mathbf{v}(\mathbf{r}) = \sum_i \mathbf{G}(\mathbf{r} - \mathbf{r_i}).\mathbf{F_i} \tag{3.4}$$

Here $\mathbf{G}(\mathbf{r} - \mathbf{r_i})$ is the Blake-Oseen tensor to a $O(h^2/d^2)$ approximation [Olm99], and is equal to:

$$G_{\alpha\beta}(r) = \frac{3h^2}{2\pi\eta}\frac{r_\alpha r_\beta}{|r|^5} \tag{3.5}$$

Here $\alpha, \beta = x, y$; h is the depth of the fluid, and η is the viscosity of the fluid.

Since the rotors are constrained to only rotate, only the tangential component of the force will affect the velocity of an individual rotor. Also, we need to remove self-interaction. If there was no coupling, each i^{th} rotor would rotate with an angular velocity $\omega_{i,t}$, hence $\mathbf{v}_i = b\omega_t\mathbf{t}_i$. Introducing $\mathbf{r}_{ij} \equiv \mathbf{r}_i - \mathbf{r}_j$, and the hydrodynamic coupling due to the rest of the rotors gives,

$$|\mathbf{v}_i| = |b\omega_t\mathbf{t}_i| + (\sum_{j=1;j\neq i}^{N} \frac{3h^2}{2\pi\eta}\frac{\mathbf{r}_{ij}\mathbf{r}_{ij}}{|\mathbf{r}_{ij}|^5}.\mathbf{F}_j).\mathbf{t}_i \tag{3.6}$$

In order to write $\mathbf{F}_j$ in a simplified manner, we can invoke Stoke's law. Drag force $\mathbf{F}$ on a sphere of radius a moving through a fluid of viscosity η at a speed $\mathbf{v}$ is given by,

$$\mathbf{F} = 6\pi\eta a\mathbf{v} \tag{3.7}$$

$|\mathbf{v}|$ due to the rotor's internal force is given by $b\omega$. Writing $6\pi\eta a = \zeta$, as the Stoke's drag coefficient,

$$F_{t,n} = \zeta b\omega_{t,n} \tag{3.8}$$

Substituting $\mathbf{v}$ from Eq.(3.2) and Eq.(3.8) into Eq.(3.6), and cancelling b from both sides gives,

$$\frac{d\phi_i}{dt} = \omega_t + \sum_{j\neq i} \frac{3h^2\zeta}{2\pi\eta} \frac{\mathbf{r}_{ij}\mathbf{r}_{ij}}{|\mathbf{r}_{ij}|^5}\omega.\mathbf{t}_i$$

Breaking ω in radial and tangential components, and writing $h^2\zeta/\eta = \gamma$, the hydrodynamic coupling constant (analogies to Kuramoto Model [Kur03]), the equation can be written as:

$$\frac{d\phi_i}{dt} = \omega_t + \sum_{j\neq i} \frac{3\gamma}{2\pi} \frac{\mathbf{r}_{ij}\mathbf{r}_{ij}}{|\mathbf{r}_{ij}|^5}(\omega_n\mathbf{n}_j + \omega_t\mathbf{t}_j).\mathbf{t}_i \tag{3.9}$$

This is the dynamical equation for how ϕ_i changes with time. It can be further simplified by introducing $\delta = \tan^{-1}(\omega_t/\omega_n)$, and $|\omega| = \sqrt{\omega_n^2 + \omega_t^2}$.

$$\frac{d\phi_i}{dt} = \omega_t + \sum_{j\neq i} \frac{3\gamma}{2\pi} \frac{1}{|\mathbf{r}_{ij}|^3}(|\omega|\cos(\delta)(\cos\phi_j, \sin\phi_j) + |\omega|\sin(\delta)(-\sin\phi_j, \cos\phi_j)).\mathbf{t_i}$$

$$\implies \frac{d\phi_i}{dt} = \omega_t + \frac{3\gamma|\omega|}{2\pi} \sum_{j\neq i} \frac{1}{|\mathbf{r}_{ij}|^3}(\cos\delta\cos\phi_j - \sin\delta\sin\phi_j, \cos\delta\sin\phi_j + \sin\delta\cos\phi_j).(-\sin\phi_i, \cos\phi_i)$$

$$\implies \frac{d\phi_i}{dt} = \omega_t + \frac{3\gamma|\omega|}{2\pi} \sum_{j\neq i} \frac{1}{|\mathbf{r}_{ij}|^3}(\cos(\delta+\phi_j)(-\sin\phi_i) + \sin(\delta+\phi_j)\cos(\phi_i))$$

$$\implies \frac{d\phi_i}{dt} = \omega_t + \frac{3\gamma|\omega|}{2\pi} \sum_{j\neq i} \frac{1}{|\mathbf{r}_{ij}|^3}\sin(\delta+\phi_j-\phi_i) \tag{3.10}$$

3.2 Simulation

The simulation was performed for a 50×50 lattice. Larger lattice sizes took much longer time to run with the available computing resources. The differential equation Eq.(3.10) is solved via Euler method with time-step, $t = 0.1$. The rotor arm length is $b = 0.1$, and distance between the rotors is $d = 1$. The coupling constant is taken to be $\gamma = 0.5$. The value of $|\omega|$ is taken to be 0.1. The initial angular position of the rotors was uniformly distributed.

3.3 Results

3.3.1 $\delta = 0°$

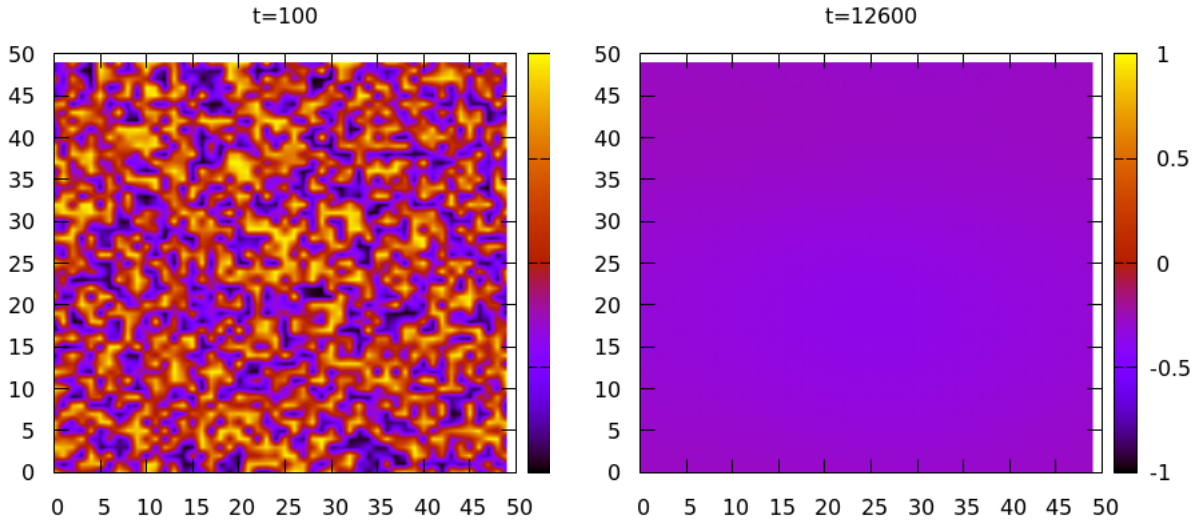

Figure 3.2: Snapshots of the rotors for $\delta = 0°$. The color range shows the value of $\cos\phi_i$, with black for -1 to yellow for +1.

For $\delta = 0°$, the force due to the rotors on the fluid is completely radial. The rotors initially start from random orientations (distributed uniformly), just pumping into the fluid, without any rotation. These rotors can be termed as "pumping-driven rotors". The movement of the rotors is solely driven by the fluid flow generated by the remaining rotors. The rotors globally synchronize after ≈ 12000 time-steps.

3.3.2 $\delta = 30°$

For $\delta = 30°$, the rotors are both pumping and torque driven. Each rotor exerts a force $\omega \cos 30° \times (\zeta b)$ on its surrounding fluid, and rotates with an angular velocity

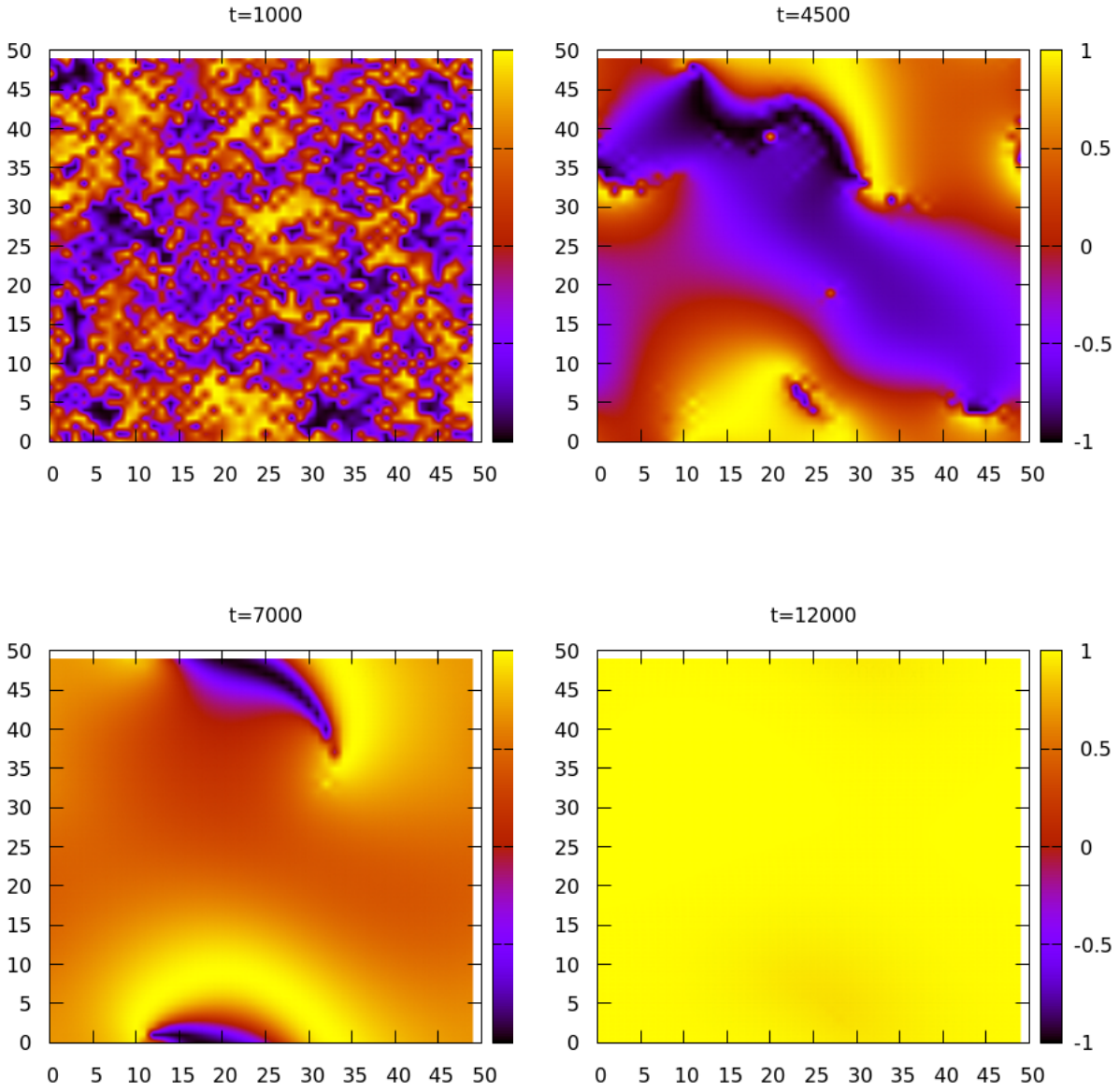

Figure 3.3: Snapshots for $\delta = 30°$.

$\omega \sin 30°$ initially. The movement of the rotors starts off only due to the individual rotor's tangential force, and then the fluid flow influences it. As in the previous case, this leads to neighbouring areas getting synchronised, seen for $t = 4500$ and $t = 7000$ in Fig.(3.3). All the rotors get globally synchronised and start rotating together as a single unit after ≈ 12000 time-steps.

3.3.3 $\delta = 60°$

Even for this case, the rotors are both torque and pumping driven. The angular velocity becomes $\omega \sin 60°$, and the radial force on the fluid is $\omega \cos 60°$. Here the

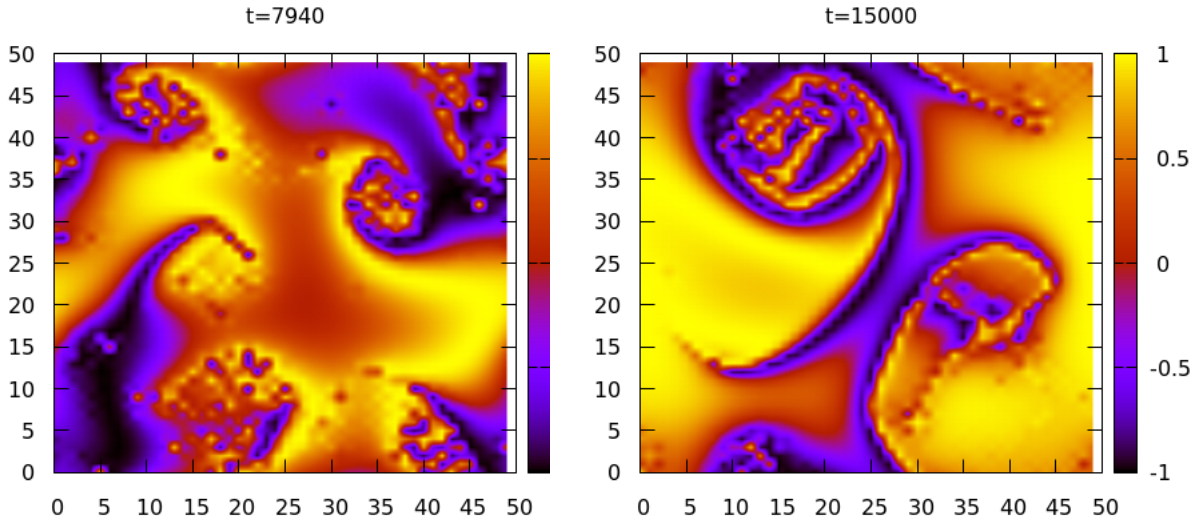

Figure 3.4: Snapshots of the angular rotors for $\delta = 60°$.

rotors don't completely synchronise, but instead form spiral waves in the fluid flow. The spirals appear to be pair based, one flowing clockwise and the other anti-clockwise. This can be seen intuitively in $t = 15000$ in Fig(3.4). The spirals spread and give rise to further spirals in the flow.

Animations for $\delta = 0°, 30°, 60°$ for a 50×50 lattice, and $\delta = 60°$ for a 100×100 lattice can be seen in this link. The spiral waves proliferation are better seen in 100×100 lattice, but the code takes a long time to simulate with the given computational resources. Hence this lattice size wasn't chosen for the other values of δ.

3.3.4 Order Parameters

A Vicsek Model [Vic+95] inspired Order Parameter was taken,

$$< n >= \frac{1}{N} | \sum_{i=1}^{N} \mathbf{n}_i | \tag{3.11}$$

$< n >$ is plotted for various values of δ in Fig.(3.5). Up until, $\delta = 50°$, the system reaches a completely steady synchronized state. The order-parameter does not reach 1 (does not get completely synchronised) for $\delta = 55°, 60°$. Spirals were shown for $\delta = 60°$ in Fig.(3.4). Hence there should exist a critical degree of frustration, $50° < \delta_c \leq 55°$ for a 50×50 lattice. The order parameters have been plotted till $t = 20000$. Steady states are not reached for $\delta = 55°, 60°$. For $\delta = 90°$, the rotors are only torque driven

and the fluid flow remains completely disordered.

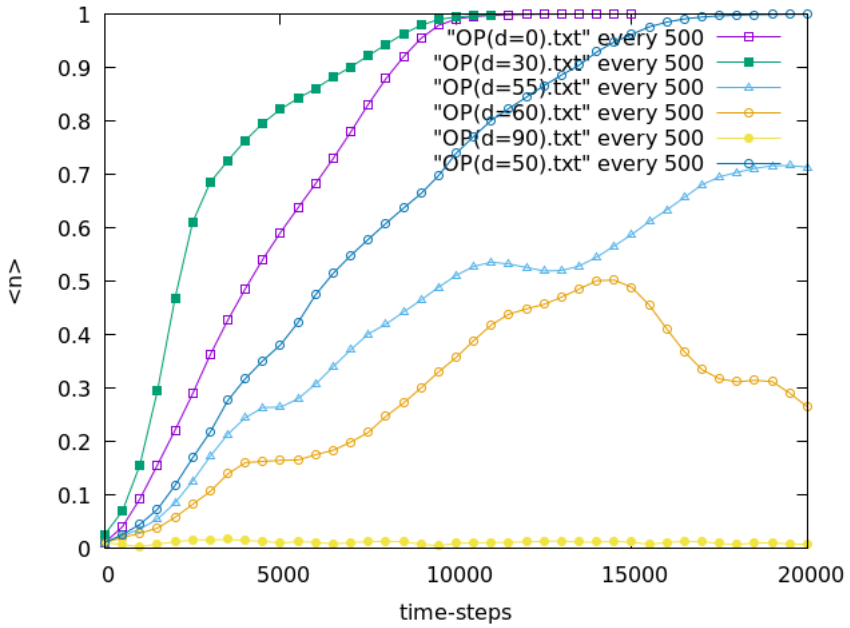

Figure 3.5: Order Parameters for various values of δ(shown as d in the plot) till 20000 time-steps.

Chapter 4

Summary

In this MS-thesis I started with a one-dimensional classical XY model pushed away from equilibrium with angular momentum conserving Langevin dynamics and showed how the angular velocity distributions closely resemble the shear flow seen in non-Newtonian fluids. Four distinct flow patterns were observed: (i)Uniform flow (similar to that for Newtonian fluids), (ii) Shear Banded flow, (iii) Solid-Fluid coexistence and (iv) Slip-plane regime. Also the system was theoretically analysed leading to a constitutive relation for the rotors using mean field theory.

Next, I moved up a dimension to a two-dimensional carpet of rotors. Also, the rotors in this system could interact hydrodynamically (the rotors were placed in a fluid). The rotors could exert force on the surrounding fluid due to internal degrees of freedom. Here under maximum frustration , the rotors synchronised in direction instantly. Upon reducing the frustration, spiral were obtained in the fluid flow. The order parameters for various degrees of frustration were also plotted. Such a 2-D XY model also presents an idea for microfluidic mixers where the flow behaviour of the fluid can be changed by just tweaking the frustration in the system.

Bibliography

[Bla71] J. R. Blake. "A note on the image system for a stokeslet in a no-slip boundary". In: *Mathematical Proceedings of the Cambridge Philosophical Society* 70.2 (1971), pp. 303–310. DOI: 10.1017/S0305004100049902.

[Dar+04] Nicholas Darnton et al. "Moving fluid with bacterial carpets". In: *Biophysical journal* 86.3 (2004), pp. 1863–1870.

[Eva+15] R. M. L. Evans et al. "Classical XY Model with Conserved Angular Momentum is an Archetypal Non-Newtonian Fluid". In: *Phys. Rev. Lett.* 114 (13 Apr. 2015), p. 138301. DOI: 10.1103/PhysRevLett.114.138301. URL: https://link.aps.org/doi/10.1103/PhysRevLett.114.138301.

[Haw04] M. D. Haw. "Jamming, Two-Fluid Behavior, and "Self-Filtration" in Concentrated Particulate Suspensions". In: *Phys. Rev. Lett.* 92 (18 May 2004), p. 185506. DOI: 10.1103/PhysRevLett.92.185506. URL: https://link.aps.org/doi/10.1103/PhysRevLett.92.185506.

[KD08] Kapilanjan Krishan and Michael Dennin. "Viscous shear banding in foam". In: *Phys. Rev. E* 78 (5 Nov. 2008), p. 051504. DOI: 10.1103/PhysRevE.78.051504. URL: https://link.aps.org/doi/10.1103/PhysRevE.78.051504.

[Kos74] J M Kosterlitz. "The critical properties of the two-dimensional xy model". In: *Journal of Physics C: Solid State Physics* 7.6 (Mar. 1974), pp. 1046–1060. DOI: 10.1088/0022-3719/7/6/005. URL: https://doi.org/10.1088/0022-3719/7/6/005.

[Kun+12] Itsuki Kunita et al. "Shear Banding in an F-Actin Solution". In: *Phys. Rev. Lett.* 109 (24 Dec. 2012), p. 248303. DOI: 10.1103/PhysRevLett.109.248303. URL: https://link.aps.org/doi/10.1103/PhysRevLett.109.248303.

[Kur03] Yoshiki Kuramoto. *Chemical oscillations, waves, and turbulence*. Chemistry Series. originally published: Springer Berlin, New York, Heidelberg, 1984. Dover Publications, 2003. ISBN: 978-0-486-42881-9.

[LG85] D. H. Lee and G. Grinstein. “Strings in two-dimensional classical XY models”. In: *Phys. Rev. Lett.* 55 (5 July 1985), pp. 541–544. DOI: 10.1103/PhysRevLett.55.541. URL: https://link.aps.org/doi/10.1103/PhysRevLett.55.541.

[Mat84] Daniel C. Mattis. “Transfer matrix in plane-rotator model”. In: *Physics Letters A* 104.6 (1984), pp. 357–360. ISSN: 0375-9601. DOI: https://doi.org/10.1016/0375-9601(84)90816-8. URL: https://www.sciencedirect.com/science/article/pii/0375960184908168.

[Olm99] Peter D Olmsted. “Two-state shear diagrams for complex fluids in shear flow”. In: *EPL (Europhysics Letters)* 48.3 (1999), p. 339.

[SMC03] Jean-Baptiste Salmon, Sébastien Manneville, and Annie Colin. “Shear banding in a lyotropic lamellar phase. I. Time-averaged velocity profiles”. In: *Phys. Rev. E* 68 (5 Nov. 2003), p. 051503. DOI: 10.1103/PhysRevE.68.051503. URL: https://link.aps.org/doi/10.1103/PhysRevE.68.051503.

[TT95] John Toner and Yuhai Tu. “Long-Range Order in a Two-Dimensional Dynamical XY Model: How Birds Fly Together”. In: *Phys. Rev. Lett.* 75 (23 Dec. 1995), pp. 4326–4329. DOI: 10.1103/PhysRevLett.75.4326. URL: https://link.aps.org/doi/10.1103/PhysRevLett.75.4326.

[UG10] Nariya Uchida and Ramin Golestanian. “Synchronization and Collective Dynamics in a Carpet of Microfluidic Rotors”. In: *Phys. Rev. Lett.* 104 (17 Apr. 2010), p. 178103. DOI: 10.1103/PhysRevLett.104.178103. URL: https://link.aps.org/doi/10.1103/PhysRevLett.104.178103.

[Vic+95] Tamás Vicsek et al. “Novel type of phase transition in a system of self-driven particles”. In: *Physical review letters* 75.6 (1995), p. 1226.

Appendix A

C code for 1-D chain of rotors

```c
#include <stdio.h>
#include <math.h>
//ran1 and gasdev

float gasdev(long *idum)
{
  float ran1(long *idum);
  static int iset=0;
  static float gset;
  float fac,rsq,v1,v2;

  if (*idum < 0) iset=0;
  if  (iset == 0) {
    do {
      v1=2.0*ran1(idum)-1.0;
      v2=2.0*ran1(idum)-1.0;
      rsq=v1*v1+v2*v2;
    } while (rsq >= 1.0 || rsq == 0.0);
    fac=sqrt(-2.0*log(rsq)/rsq);
    gset=v1*fac;
    iset=1;
    return v2*fac;
  } else {
    iset=0;
    return gset;
  }
}

// ran1 from Numerical Recipes C with uniform Distribution

#define IA 16807
#define IM 2147483647
#define AM (1.0/IM)
```

```
#define IQ 127773
#define IR 2836
#define NTAB 32
#define NDIV (1+(IM-1)/NTAB)
#define EPS 1.2e-7
#define RNMX (1.0-EPS)

float ran1(long *idum)
{
  int j;
  long k;
  static long iy=0;
  static long iv[NTAB];
  float temp;

  if (*idum <= 0 || !iy) {
    if (-(*idum) < 1) *idum=1;
    else *idum = -(*idum);
    for (j=NTAB+7;j>=0;j--) {
      k=(*idum)/IQ;
      *idum=IA*(*idum-k*IQ)-IR*k;
      if (*idum < 0) *idum += IM;
      if (j < NTAB) iv[j] = *idum;
    }
    iy=iv[0];
  }
  k=(*idum)/IQ;
  *idum=IA*(*idum-k*IQ)-IR*k;
  if (*idum < 0) *idum += IM;
  j=iy/NDIV;
  iy=iv[j];
  iv[j] = *idum;
  if ((temp=AM*iy) > RNMX) return RNMX;
  else return temp;
}
//end


double theta[1024],ang_vel[1024], avg[1024];
long seed;
double r,p,q; //var in acc
double mu, T, gsr;//parameters: gsr=global shear rate
double acc(int k, double a, double v) //acceleration function
{
    p=sin(theta[k+1]-a)+mu*(ang_vel[k+1]-v)+r*gasdev(&seed);
    q=sin(a-theta[k-1])+mu*(v-ang_vel[k-1])+r*gasdev(&seed);
    return(p-q);
```

```
}
int main()
{
    int n=1024;
    seed= -1234;
    int i,j; //loop var
    int c=0; //counter var
    mu=10;
    T=0.02;
    gsr=0.0078;
    r=sqrt(2*mu*T);
    double evol=450000; // time until which system is evolved
    double t=0., dt=0.01; //time var, increment
    double dx1,dx2,dx3,dx4,dv1,dv2,dv3,dv4,dx,dv; //RK4 vars

    FILE *fpr= fopen("shb_pot1.txt","w");
    FILE *gpr= fopen("EHSW_shb.txt","w");

    for (i=0;i<n;i++) //initialising
    {
        theta[i]=0.;
        ang_vel[i]=0.;
    }
    ang_vel[0]=-n*gsr/2; //initial twist
    ang_vel[n-1]=n*gsr/2;
    for(i=0;i<500000;i++)
    {
        theta[0]=theta[0]+dt*ang_vel[0];
        theta[n-1]=theta[n-1]+dt*ang_vel[n-1];
        for(j=1;j<n-1;j++) //RK4
        {
            dx1=dt*ang_vel[j];
            dv1=dt*acc(j,theta[j],ang_vel[j]);
            dx2=dt*(ang_vel[j]+dv1/2);
            dv2=dt*acc(j,theta[j]+dx1/2,ang_vel[j]+dv1/2);
            dx3=dt*(ang_vel[j]+dv2/2);
            dv3=dt*acc(j,theta[j]+dx2/3,ang_vel[j]+dv2/3);
            dx4=dt*(ang_vel[j]+dv3);
            dv4=dt*acc(j,theta[j]+dx3,ang_vel[j]+dv3);
            dx=(dx1+2*dx2+2*dx3+dx4)/6;
            dv=(dv1+2*dv2+2*dv3+dv4)/6;
            theta[j]=theta[j]+dx;
            ang_vel[j]=ang_vel[j]+dv;

        }

        if (i>499500)//inter rotor potential plots
```

```
128         {
129             for(j=1;j<n;j++)
130             {
131                 fprintf(fpr,"%d\t%d\t%lf\n",j,i,-cos(theta[j]-theta[j
    -1]));
132             }
133         }
134 
135         if(i==evol)//averaging
136         {
137             c++;
138             for(j=0;j<n;j++)
139             {
140                 avg[j]=avg[j]+ang_vel[j];
141             }
142             evol=evol+100;
143         }
144     }
145 
146     for(i=0;i<n;i++)
147     {
148         fprintf(gpr,"%d\t%lf\t%lf\n",i,theta[i],avg[i]);
149     }
150 }
```

Appendix B

C code for 2-D Carpet of Rotors with Hydrodynamic Interaction

```
#include <stdio.h>
#include<math.h>
#include <time.h>

//ran1
#define IA 16807
#define IM 2147483647
#define AM (1.0/IM)
#define IQ 127773
#define IR 2836
#define NTAB 32
#define NDIV (1+(IM-1)/NTAB)
#define EPS 1.2e-7
#define RNMX (1.0-EPS)

float ran1(long *idum)
{
  int j;
  long k;
  static long iy=0;
  static long iv[NTAB];
  float temp;

  if (*idum <= 0 || !iy) {
    if (-(*idum) < 1) *idum=1;
    else *idum = -(*idum);
    for (j=NTAB+7;j>=0;j--) {
      k=(*idum)/IQ;
      *idum=IA*(*idum-k*IQ)-IR*k;
      if (*idum < 0) *idum += IM;
      if (j < NTAB) iv[j] = *idum;
```

```
    }
    iy=iv[0];
  }
  k=(*idum)/IQ;
  *idum=IA*(*idum-k*IQ)-IR*k;
  if (*idum < 0) *idum += IM;
  j=iy/NDIV;
  iy=iv[j];
  iv[j] = *idum;
  if ((temp=AM*iy) > RNMX) return RNMX;
  else return temp;
}
//end

//gasdev
float gasdev(long *idum)
{
  float ran1(long *idum);
  static int iset=0;
  static float gset;
  float fac,rsq,v1,v2;

  if (*idum < 0) iset=0;
  if  (iset == 0) {
    do {
      v1=2.0*ran1(idum)-1.0;
      v2=2.0*ran1(idum)-1.0;
      rsq=v1*v1+v2*v2;
    } while (rsq >= 1.0 || rsq == 0.0);
    fac=sqrt(-2.0*log(rsq)/rsq);
    gset=v1*fac;
    iset=1;
    return v2*fac;
  } else {
    iset=0;
    return gset;
  }
}

//end
void main()
{

    clock_t begin= clock();
    //constructing 50 * 50 lattice
    int i,j,k,l;
    long seed=-12345;
```

```
79      int time;
80      double t=0., dt=0.1;
81      int n=50;
82      double phi[n][n]; //angles
83      double phi1[n][n];
84      double s; // summation term
85      double ang_diff;
86      char snum[10];
87      double avg_nx, avg_ny; //spatial average of phi
88      double director; //<n>
89      //parameters
90      double b=0.1;
91      double w=0.1; //angular frequency
92      double delta=(double)(M_PI/3); // angle of frustration
93      printf("sin delta:%lf\n",sin(delta));
94      int Time=15001; //total time
95      double gamma=0.5;//coupling constant
96
97      double distx, disty, dist; //distance x, y
98      for (i=0;i<n;i++)
99      {
100         for(j=0;j<n;j++)
101         {
102             phi[i][j]=2*M_PI*ran1(&seed);
103             phi1[i][j]=phi[i][j]; //creating a copy
104         }
105     }
106     FILE *gpr=fopen("Order Parameter.txt","w");
107     //time evolution
108     for(time=0;time<Time;time++)
109     {
110         t=t+dt;
111         avg_nx=0.;
112         avg_ny=0.;
113   for(i=n-1;i>=0;i--)
114   {
115     for(j=n-1;j>=0;j--)
116     {
117       s=0.;
118       for(k=n-1;k>=0;k--)
119       {
120         for(l=n-1;l>=0;l--)
121         {
122           if(j!=l && i!=k)
123           {
124             distx= i+b*cos(phi[i][j])-(k+b*cos(phi[k][l])); //
    calculating distance
```

```
125             if((fabs(distx))>(n/2))
126             {
127               distx=n-fabs(distx); // PBC
128             }
129             disty= j+b*sin(phi[i][j])-(l+b*sin(phi[k][l])); //
    calculating distance
130             if ((fabs(disty))>(n/2))
131             {
132               disty=n-fabs(disty); //PBC
133             }
134             dist=sqrt(distx*distx+disty*disty); //
135             ang_diff=phi[i][j]-phi[k][l]-delta; //
136             s= s+ (double)(1/(dist*dist*dist))*sin(ang_diff);
137           }
138         }
139       }
140       phi1[i][j]=phi[i][j]+w*sin(delta)*dt-((3*gamma*w)/(2*M_PI))*s*dt;
141       avg_nx=avg_nx+(double)cos(phi1[i][j])/(n*n);
142       avg_ny=avg_ny+(double)sin(phi1[i][j])/(n*n);
143     }
144   }
145
146
147         sprintf(snum, "%d.txt",time);
148         FILE *fpr=fopen(snum,"w");
149         for(i=0;i<n;i++)
150         {
151                 for (j=0;j<n;j++)
152                 {
153                     fprintf(fpr,"%d\t%d\t%lf\n",i,j,cos(phi1[i][j]));
154                     phi[i][j]=phi1[i][j];
155                 }
156     fprintf(fpr,"\n");
157         }
158
159   fclose(fpr);
160   director= sqrt(avg_nx*avg_nx+avg_ny*avg_ny);
161   fprintf(gpr,"%d\t%lf\n",time,director);
162   printf("%lf%% done.\n",(float)time/(Time-1)*100.0);
163
164
165
166
167
168     }
169     fclose(gpr);
170     clock_t end= clock();
```

```
171     printf("TIME TAKEN: %lf hours", (double)(end-begin)/(CLOCKS_PER_SEC
        *3600));
172
173 }
```